Ordering of strained islands during surface growth

Jean-Noël Aqua,* Thomas Frisch,* and Alberto Verga
Institut Matériaux Microélectronique Nanosciences de Provence, Aix-Marseille Université, UMR 6242, 13397 Marseille, France
(Received 24 September 2009; revised manuscript received 14 January 2010; published 12 February 2010)

We study the morphological evolution of strained islands in growing crystal films by use of a continuum description including wetting, elasticity, and deposition. We report different nonlinear regimes following the elastic instability and tuned by the flux. Increasing the flux, we first find an annealinglike dynamics, then a slower but nonconventional ripening followed by a steady regime, while the island density continuously increases. The islands develop spatial correlations and ordering with a narrow two-peaked distance distribution and ridgelike clusters of islands at high flux.

DOI: 10.1103/PhysRevE.81.021605 PACS number(s): 81.15.Aa, 68.55.−a, 68.35.Ct

I. INTRODUCTION

Nonequilibrium crystal growth is questioning many fundamental and experimental issues in particular in the domain of self-organization of nanostructures [1–7]. For example, quantum dots have lead to numerous applications [8] such as photovoltaic cells, memory storage, or light emission. However, the different scenario governing island formations are still challenged as regards their density, size distribution, and spatial ordering [9–11]. We focus here on the properties of islands produced in heteroepitaxy.

When a film is coherently deposited on a substrate with a lattice mismatch, it experiences an elastic stress that can be relieved by a morphological evolution. For strong enough mismatch, islands are nucleated in an abrupt two to three-dimensions transition. However, for intermediate mismatch, the evolution begins by surface diffusion with a nucleationless ripple formation [12–15] which results from an elastic instability reminiscent of the Asaro-Tiller-Grinfel'd (ATG) instability [16,17]. Contrarily to the evolution in thick films [16], no dislocations are generated in thin films where instead the ripples transform smoothly into islands separated by a wetting layer [14]. In order to go beyond the simple exponential growth description, one needs to take into account the nonlinear terms which allow to simulate island coarsening quantitatively [18–22]. The question we address in this article is the influence of the growth dynamics on the spatial organization of the islands due to the elastic instability. To tackle this problem, we use a continuum modelization of the crystal accounting both for wetting and elastic interactions. Wetting, which breaks the translational invariance in the growth direction, introduces significant flux dependence. Consequently, once diffusion proceeded and led to islands, we find different nonlinear regimes as the flux F increases. Departing from the near annealing case, island ordering arises first as clusters form. Then, for high enough fluxes, the island density is frozen and the dot density and ordering are maximum. To the best of our knowledge, this work tackles for the first time the influence of the growth dynamics (and thence of the deposition flux) on the islands produced during the ATG instability as nonlinear effects due to the boundary condition at the surface together with the wetting potential come into play.

II. CONTINUUM MODEL OF THE MORPHOLOGICAL EVOLUTION

The dynamics of a surface during crystal growth involves different mechanisms such as diffusion, attachment, or relaxation. The evolution of its surface $z=H(\mathbf{r},t)$ at position $\mathbf{r}=(x,y)$, see Fig. 1, with time t can be written as

$$\frac{\partial H}{\partial t} = \mathcal{V}[H] + a_f F, \tag{1}$$

where $\mathcal{V}[H]$ is dictated by the predominant mechanisms at stake while a_f is the film lattice parameter. In homoepitaxy, symmetry constraints enforce $\mathcal{V}$ to depend only on the slope of H [7] so that F disappears in the Galilean transformation $H(\mathbf{r},t)=Ft+h(\mathbf{r},t)$. This invariance is violated in heteroepitaxy when a film is coherently deposited on a substrate. We consider a film evolving in the Stransky-Krastanov mode, with a dynamics due to surface diffusion induced by chemical potential gradients. Hence,

$$\mathcal{V}[H] = D\sqrt{1+|\nabla H|^2}\nabla_S^2\mu, \tag{2}$$

where D is a diffusion coefficient, ∇_S, the surface gradient, and μ, the surface chemical potential given by the functional derivative $\mu=\delta(\mathcal{F}^{\mathrm{El}}+\mathcal{F}^{S})/\delta H$, where $\mathcal{F}^{S}=\int d\mathbf{r}\,\gamma(H)\sqrt{1+|\nabla H|^2}$ and $\mathcal{F}^{\mathrm{El}}$ is the elastic free energy. Wetting is embedded in the H dependence of the surface energy γ, which describes the change with H of the local environment of a particle when the film/substrate interface is present [23], and which precisely breaks translational invariance in

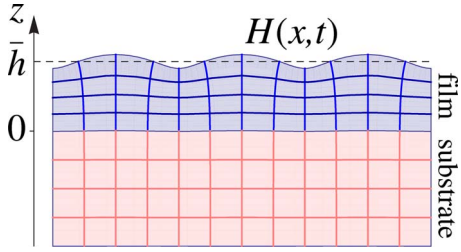

FIG. 1. (Color online) Sketch of the film/substrate geometry.

*Also at École Centrale Marseille.

the z direction. Note that neither alloying nor anisotropy are considered here, which can prove significant in some experimental regimes, see e.g., [2,4,24–27].

To set scales, we choose to depict a $Ge_{0.25}Si_{0.75}$-like film deposited on a Si substrate with a reference lattice with a substrate (film) lattice parameter $a_s=0.27$ nm ($a_f=1.01$ a_s). Surface diffusion is given by $D=D_s \exp[-\Delta E_d/k_BT]a_f^4/k_BT$ with $\Delta E_d=0.83$ eV and $D_s=8.45$ 10^{-10} m^2/s, see e.g., [17], and the working temperature is 700 °C. The film surface energy is $\gamma_f=1.3$ J/m^2 and we extrapolate *ab initio* calculations for Si/Ge systems [28] by considering $\gamma(h)=\gamma_f[1+c_w \exp(-h/\delta)]$ where $\delta=a_f$ and $c_w=0.09$. The characteristic length and time scales that will be used below are then $l_0=\gamma_f/2(1+\nu_f)\mathcal{E}^0$ and $t_0=l_0^4/D\gamma_f$, where $\mathcal{E}^0=E_f\eta^2/(1-\nu_f)$ is an elastic energy density involving the film Poisson ratio ν_f and film Young modulus E_f together with the film/substrate mismatch $\eta=(a_f-a_s)/a_s$. The numerical values concerning a $Ge_{0.25}Si_{0.75}$-like film are then $l_0=27$ nm and $t_0=25$ s. On these time and length scales, the deposition and diffusion noise [7,29] which can be implemented in Eq. (1), are in fact not relevant and were not considered.

Mechanical equilibrium is supposed to be achieved on time scales faster than the system evolution, which enforce the Lamé equations $\partial_q\sigma_{pq}=0$ to be valid in the film and substrate. The stress tensor σ_{pq} is a linear function of the strain tensor

$$e_{pq}=\frac{1}{2}(\partial_q u_p+\partial_p u_q)-e^r_{pq}, \tag{3}$$

where $\mathbf{u}$ is the displacement with respect to the substrate reference state. The reference strain is

$$e^r_{pq}=(1-a_f/a_s)\delta_{pq}(\delta_{px}+\delta_{qy}), \tag{4}$$

in the film and 0 otherwise, where δ_{pq} is the Kronecker symbol with $p,q=x,y,z$. Although anisotropy is certainly relevant, our first concern here is on the influence of a deposition flux on the dynamics of stressed films. Different sources of anisotropy are revealed by experiments, which appeal for specific examination out of the scope of the present paper. Hence, to simplify the model, we consider isotropic elasticity, where strains and stresses are related through

$$\sigma_{ij}=\frac{E_f}{1+\nu_f}\left[e_{ij}+\frac{\nu_f}{1-2\nu_f}e_{ll}\delta_{ij}\right]. \tag{5}$$

Furthermore, we consider identical film and substrate elastic constants as experiments usually involve materials with similar constants. Different elastic constants could only change significantly the second order in the asymptotic expansion that we develop below, but by an extra small factor proportional to the difference in these constants. The Lamé equations are then solved using Fourier transforms with respect to the two-dimensional position $\mathbf{r}$, $\mathcal{F}[h]=(2\pi)^{-2}\int d\mathbf{r}e^{i\mathbf{k}\cdot\mathbf{r}}h(\mathbf{r})$, where $\mathbf{k}=(k_x,k_y)$, with the following boundary conditions: the film/substrate interface is coherent with continuous stresses and the film/vacuum surface is free, with a negligible surface stress. Hence, we impose

$$\mathbf{u}(\mathbf{r},z=0^-)=\mathbf{u}(\mathbf{r},z=0^+), \tag{6}$$

$$\boldsymbol{\sigma}\cdot\mathbf{z}(\mathbf{r},z=0^-)=\boldsymbol{\sigma}\cdot\mathbf{z}(\mathbf{r},z=0^+), \tag{7}$$

$$\boldsymbol{\sigma}\cdot\mathbf{n}[\mathbf{r},z=H(\mathbf{r})]=0, \tag{8}$$

where $\mathbf{z}$ is the normal to the film/substrate interface, while $\mathbf{n}$ is the normal to the film surface. To solve the last boundary condition, we use here the small-slope approximation amenable for arbitrary deposited thicknesses, which is not the same set of approximation as the thin film approximation used in Ref. [21]. The present small-slope approximation is relevant for the growth case where the mean film height is arbitrarily thick. Defining $\bar{h}$ as the spatial average of H, see Fig. 1, we suppose that the film surface is characterized by a shallow modulation where $H-\bar{h}$ is small compared to the instability wavelength computed below which is of order of the characteristic length l_0, ratio of the surface energy to the misfit elastic energy density; hence, we decompose H using a small parameter ε as

$$H(\mathbf{r},t)=\bar{h}(t)+\varepsilon h(\mathbf{r},t). \tag{9}$$

We thus obtain the displacements $\mathbf{u}$ as series of ε up to second order, $\mathbf{u}=\Sigma_{n=0}^2\varepsilon^n\mathbf{u}^{(n)}$, where

$$\mathbf{u}^{(0)}=[0,0,2\eta\nu_f z/(1-\nu_f)]. \tag{10}$$

At first order, one gets

$$u_x^{(1)}(\mathbf{k},z)=\frac{\eta(1+\nu_f)e^{|\mathbf{k}|(z-\bar{h})}}{1-\nu_f}\times ik_x[|\mathbf{k}|(z-\bar{h})+2(1-\nu_f)]h(\mathbf{k})/|\mathbf{k}|, \tag{11}$$

and with a similar expression for the y component after x and y exchange, while the z component is given by

$$u_z^{(1)}(\mathbf{k},z)=\frac{\eta(1+\nu_f)e^{|\mathbf{k}|(z-\bar{h})}}{1-\nu_f}\times[1-2\nu_f-|\mathbf{k}|(z-\bar{h})]h(\mathbf{k}), \tag{12}$$

see e.g., [30] in the case of identical film and substrate elastic constants. As a consequence of the nonlinearity enforced by the boundary condition (8), the displacements involve convolutions of the film height $h(\mathbf{k})$. We find

$$u_x^{(2)}(\mathbf{k},z)=\frac{i\eta(1+\nu_f)e^{|\mathbf{k}|(z-\bar{h})}}{(1-\nu_f)|\mathbf{k}|^3}\int d\mathbf{k}_1\frac{h(\mathbf{k}_1)h(\mathbf{k}-\mathbf{k}_1)}{|\mathbf{k}_1|}\times\{k_x(z-\bar{h})|\mathbf{k}|[|\mathbf{k}||\mathbf{k}_1|\mathbf{k}\cdot\mathbf{k}_1-2(\mathbf{k}\cdot\mathbf{k}_1)^2-2\nu_f(\mathbf{k}\wedge\mathbf{k}_1)^2]+(1-2\nu_f)k_x|\mathbf{k}||\mathbf{k}_1|\mathbf{k}\cdot\mathbf{k}_1-4(1-\nu_f)[k_{1,x}|\mathbf{k}|^2\mathbf{k}\cdot\mathbf{k}_1+\nu_f k_x(\mathbf{k}\wedge\mathbf{k}_1)^2]\}, \tag{13}$$

with a similar expression for $u_y^{(2)}$ after the exchange of x and y. Finally, the last component $u_z^{(2)}$ is given by

$$u_z^{(2)}(\mathbf{k},z) = \frac{\eta(1+\nu_f)e^{|\mathbf{k}|(z-\bar{h})}}{(1-\nu_f)|\mathbf{k}|^3}\int d\mathbf{k}_1 \frac{h(\mathbf{k}_1)h(\mathbf{k}-\mathbf{k}_1)}{|\mathbf{k}_1|} \times \{(z-\bar{h})|\mathbf{k}|^2[2(\mathbf{k}\cdot\mathbf{k}_1)^2 + 2\nu_f(\mathbf{k}\wedge\mathbf{k}_1)^2 - |\mathbf{k}| \times|\mathbf{k}_1|\mathbf{k}\cdot\mathbf{k}_1] + 2(1-\nu_f)\mathbf{k}^2|\mathbf{k}_1|\mathbf{k}\cdot\mathbf{k}_1 - 2(1-2\nu_f)|\mathbf{k}| \times[(\mathbf{k}\cdot\mathbf{k}_1)^2 + \nu_f(\mathbf{k}\wedge\mathbf{k}_1)^2]\}. \quad (14)$$

Given the expression of $\mathbf{u}$ up to second order in ε, we are then in a position to compute at order ε^2 the elastic contribution μ^{El} which is the elastic energy density evaluated at the film surface,

$$\mu^{\mathrm{El}}(\mathbf{r},t) = \frac{1}{2}\sigma_{pq}e_{pq}|_{z=H(\mathbf{r},t)}, \quad (15)$$

which after some calculation reduces to

$$\frac{\mu^{\mathrm{El}}}{\mathcal{E}_0} = 1 - \mathcal{H}_{xx}[h] - \mathcal{H}_{yy}[h] + 2h\Delta h + |\nabla h|^2 + \mathcal{H}_{xx}[h(\mathcal{H}_{xx}[h] + \nu_f\mathcal{H}_{yy}[h])] + 2(1-\nu_f)\mathcal{H}_{xy}[h\mathcal{H}_{xy}[h]] + \mathcal{H}_{yy}[h(\mathcal{H}_{yy}[h] + \nu_f\mathcal{H}_{xx}[h])] + \frac{1}{2}\mathcal{H}_{xx}[h]^2 + \frac{1}{2}\mathcal{H}_{yy}[h]^2 + (1-\nu_f)\mathcal{H}_{xy}[h]^2 + \nu_f\mathcal{H}_{xx}[h]\mathcal{H}_{yy}[h], \quad (16)$$

where we define the generalized Hilbert transform

$$\mathcal{H}_{ij}[h] = \mathcal{F}^{-1}\{(k_ik_j/|\mathbf{k}|)\mathcal{F}[h]\}, \quad (17)$$

with indices running over x and y. Eventually, considering $\bar{h}=a_fFt$ which cancels out the second term of the right-hand side of Eq. (1), we find the dynamical equation

$$\frac{\partial h}{\partial t} = \Delta\left\{-(1+c_we^{-(h+\tilde{F}t)/\delta})\Delta h - \frac{c_w}{\delta}\frac{e^{-(h+\tilde{F}t)/\delta}}{\sqrt{1+|\nabla h|^2}} - \mathcal{H}_{ii}(h) + 2h\Delta h + |\nabla h|^2 + 2\mathcal{H}_{ij}[h\theta_{ijkl}\mathcal{H}_{kl}(h)] + \mathcal{H}_{ij}(h)\theta_{ijkl}\mathcal{H}_{kl}(h)\right\}, \quad (18)$$

where ε is set to 1, $\tilde{F}=a_fFt_0/l_0$ and summation over repeated indices. The long-range elastic interactions enforce the nonanalyticity in the operator $\mathcal{H}_{ij}[h]$ and introduce nonlocal effects in the dynamical Eq. (18). The nonlinear terms are given with $\theta_{ijij}=1$, $\theta_{iijj}=-\theta_{ijji}=\nu_f$ when $i\neq j$ and 0 otherwise. It is worthwhile to realize that a lone term $h\Delta h$ in the right-hand side of (18) would be ruled out by symmetry considerations [7] but is allowed here when put in balance with the nonlocal nonlinear terms. Indeed, taking into account both local and nonlocal terms ensure the invariance of the elastic energy under the Galilean transformation $h\rightarrow h+\bar{h}(t)$ for arbitrary $\bar{h}(t)$, which is a consequence of the hypothesis of equal film and substrate elastic constants. Accordingly, the dependence on $\bar{h}(t)$ will appear in the following exclusively as a consequence of the dependence of $\gamma(h)$ on h which breaks translational invariance.

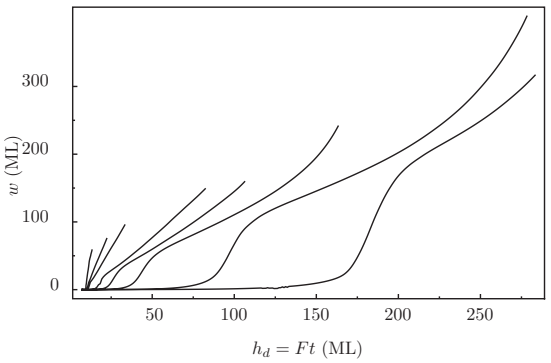

FIG. 2. Simulation of the roughness evolution resulting from Eq. (18) with the deposited height for, from left to right, $F=10^{-4},5\times10^{-4},10^{-3},5\times10^{-3},10^{-2},2\times10^{-2},5\times10^{-2},10^{-1}$ ML/s.

III. NUMERICAL RESULTS: ISLAND FORMATION, COARSENING, AND ORDERING

A. Instability and roughening

We performed numerical simulations of Eq. (18) using a pseudospectral method. We consider an initial roughness of amplitude 1 monolayer (ML) given by a random profile. The initial film height is $\bar{h}_0(t=0)=7$ ML just below the elastic instability threshold $h_c\simeq 8.2$ ML defined below. Similarly to the annealing case [21], the simulations reveal that the combination of wetting and nonlinear nonlocal elastic terms prevents the finite-time singularities, which in thick films, lead to dislocations [16]. In addition, we find that the system evolution depends strongly on the deposition flux. Different curves of the roughness $w=[\langle h^2\rangle-\langle h\rangle^2]^{1/2}$ as function of the deposited height $h_d=Ft$ are depicted in Fig. 2 for different fluxes. The roughness first increases exponentially in a linearlike dynamics. After a first inflexion point, the system enters a first nonlinear stage where $w\sim t$, and after a second one, displays a faster than linear roughness increase. The deposited heights corresponding to these inflexions increase linearly with the flux, though the different curves cannot be rescaled on a single one, signaling different ripening mechanisms depending on the flux.

To evaluate the time of emergence of the islands, we define a dynamical critical height $h_s(F)$ after which w is greater than $w_s=3$ ML. It is well fitted by an affine law $h_s=10+1200F$ (ML) with a limit at low flux greater than h_c due to the threshold present in the definition of h_s. The values of h_s obtained here for $T=700$ °C differ from the smaller values of the apparent critical thickness derived with the analysis of Ref. [17]. The latter is defined via a comparison of relative growth rates, whereas h_s is defined here directly from the roughness which is independent of the reference frame. The dynamical critical height h_s is related to the growth in the linear regime and can be roughly estimated. In the linear approximation, h small, the evolution of Eq. (18) can be reformulated in Fourier space as

$$h(\mathbf{k};t) = h(\mathbf{k};t_0)\exp\left[\int_{t_0}^{t} ds\,\sigma(\mathbf{k};\bar{h}_0+\tilde{F}s)\right], \quad (19)$$

where

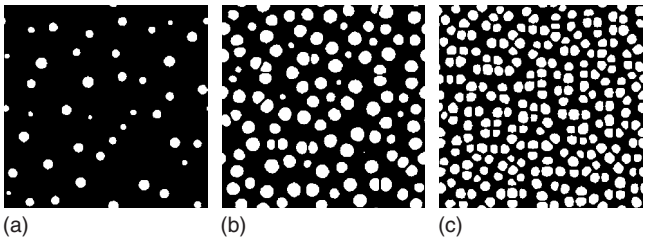

FIG. 3. Typical island configurations in the nonlinear regime for $F=$(a) 10^{-4}, (b) 10^{-2}, and (c) 10^{-1} ML/s in a 128 $l_0 \times 128$ l_0 system (the snapshots correspond respectively to $h_d=13$, 105, and 283 ML).

$$\sigma(\mathbf{k};\bar{h}) = -k^2 c_w e^{-\bar{h}/\delta}/\delta^2 + |k|^3 - k^4(1 + c_w e^{-\bar{h}/\delta}). \quad (20)$$

By definition of h_c, σ is negative for $\bar{h}<h_c$ and otherwise positive in a $\bar{h}$-dependent k interval. To estimate h_s, we consider an initial undulation with wavevector k_* and an initial amplitude $h_{1,0}=1$ ML. We can solve exactly for $h_1^*(\mathbf{r};t)$ and the critical deposited height and find

$$h_s^*(F) = \xi + \delta W[-3c_w(1+k_*^2\delta^2)\exp(-\xi/\delta)/k_*^2\delta^2], \quad (21)$$

with the product-log function W and the length

$$\xi = \bar{h}_0 + 4c_w(1+k_*^2\delta^2)e^{-\bar{h}_0/\delta}/k_*\delta + F\log(w_s/h_{1,0})/k_*^4.$$

Considering $k_*=0.35$, the solution is well fitted by $h_s^*(F)=10+1300F$ (ML) which is a rough estimate of h_s for the full equation at low flux. Similarly to the numerical results, h_s^* increases nearly linearly with F in the regime of parameters studied here. Also, the limit at low fluxes is greater than the instability critical height h_c due to the threshold in the definition of h_s. These results could be compared to experiments investigating the appearance of islands as function of the ratio D/F.

B. Nonlinear regimes

Above the critical height, the system enters the nonlinear stage where islands, surrounded by a wetting layer, grow both by deposition and coarsening, see Fig. 3. Then, depending on the flux, we find different nonlinear regimes that we will described below. Hence, the island density ρ is plotted in Fig. 4 for different fluxes. Islands appear all the later that the flux is high, as a result of the competition between diffusion and deposition. In addition, the dynamics depends strongly on the flux. At low flux, the island density is convex, similarly to the annealing case, when the system has time to coarsen by surface diffusion. However, in the intermediate regime for F in between F_1 and F_2 with $F_1 \simeq 10^{-2}$ ML/s and $F_2 \simeq 5\ 10^{-2}$ ML/s, the density evolution becomes concave, whereas in the steady regime, $F>F_2$, the island density is constant in a large time interval. The values of F_1 and F_2 depend on the temperature and the details of the wetting that are set here with typical coefficients. In all regimes, the island density at a given coverage is an increasing function of the flux and saturates at a value limited by the instability wavelength, which indicates a route for controlling island densities experimentally.

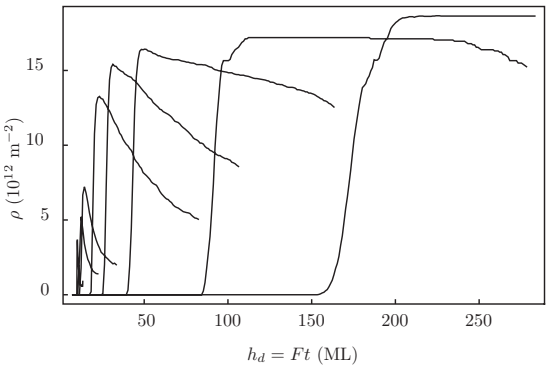

FIG. 4. Island density as function of the deposited height with, from left to right, the fluxes of Fig. 2.

At this point, we stress the difference between the flux dependence that we report here for the elastic instability with the one already observed during experiments investigating island nucleation [31,32]. The different nonlinear regimes occur on time scales much larger than the diffusion time scale t_0 so that the flux dependence in the present work is *not* similar to the competition between diffusion and deposition at stake for island nucleation. In the island nucleation regime, this competition leads to two-dimensional (2D) island precursors which sizes and densities depend on the time to form nuclei compared to the time of arrival of new material, see e.g., Ref. [33]. Hence, the very early stages of island nucleation depend crucially on the deposition flux. On the contrary, the elastic instability always begins with the same stage characterized by an undulation with a wavelength maximizing the growth rate. The flux dependence occurs only after this undulation transformed into well-defined island which then coarsen differently depending on the flux. Hence, the stricking similarity between Fig. 1 of Ref. [32] and the different morphologies that we display in Fig. 3 is not to be overestimated.

The change in dynamics from a convex island density evolution in the annealinglike case to a concave one for growing films is similar to the results of the experiments by Floro and co-workers [15] where the negativeness of $d^2\rho/dt^2$ is signaling a non standard ripening. Indeed, a typical coarsening dynamics tends to decrease its driving force resulting in a damped evolution. A faster dynamics can nevertheless be apprehended within a mean-field approach describing the island size distribution evolution due to chemical potentials accounting for elastic interactions [15]. These long-range interactions are precisely the central ingredient of Eq. (18) which can lead to such a dynamics when coupled with deposition growth and our simulations exhibit a regime where this concave evolution is to be expected. Moreover, in all regimes, the dot density evolution is slowed down even when it is given as a function of the instability time scale instead of the deposited height. Hence, even if a wetting layer has developed and allows surface diffusion, the stabilization of the islands results from an effective weakening of surface diffusion currents when deposition is present.

To give more quantitative information on the coarsening in this system, we computed the island coverage θ together with the mean island volume, see Figs. 5 and 6. Similarly to

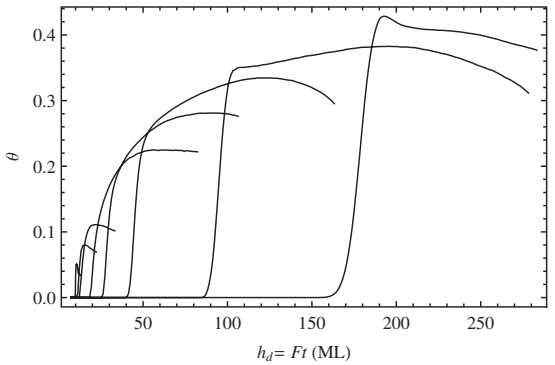

FIG. 5. Island coverage as function of the deposition height with the same convention as in Fig. 2.

the experiments of [15], we find that the mean island volume increases faster than the linear growth characteristic of deposition and that the island coverage increases with a concave evolution. In the steady regime $F > F_2$, the decrease in the island coverage at constant island density, see Fig. 4, signals a narrowing of the island base as elastic relaxation in an isotropic film is more efficient for high aspect ratio islands. On the other hand, the faster than linear increase in the mean island volume seems associated to island decimation and is indeed correlated with the decrease in the island density.

C. Island ordering

The different nonlinear regimes are moreover characterized by different spatial organization, see Fig. 3. At low flux, the islands do not exhibit strong spatial correlations, similarly to the annealing case [21], while for higher flux, island decimation, driven by surface diffusion, leads to the emergence of island clusters. These clusters, absent in the annealing case, involve more and more islands as F increases (Fig. 3). To quantify these correlations, we first assign an area mass center to each island and construct a Delaunay triangulation for this set of points. The typical nearest-neighbor distance histograms in the nonlinear regimes are then plotted in Fig. 7. At low flux in Fig. 7(a), the histogram displays a broad bell shape with a modulation reminiscent of the instability initial stages, where, beside the first peak near the initial wavelength $\lambda \simeq 20\ l_0$, the other peaks arise as coarsening is fully developed. For intermediate flux in Fig. 7(b), the histogram is significantly narrowed with a main peak near λ and other peaks which position increase slightly with time as island decimation occurs. The first small peak around $d=15$ arises at a distance smaller than λ and reveals the appearance of island pairing. In the steady high flux regime, Fig. 7(c), ordering is maximal and is described by a narrow distance distribution with two peaks related to the typical distance between two islands in a cluster and between clusters. The first peak already observed at intermediate flux arises at a position significantly lower than the instability wavelength λ, signaling a narrowing of the distance between mass centers during clustering at high flux, while the second peak sticks at λ. In this case, a particular ordering is observed in Fig. 3(c) as islands self-organize in ridgelike patterns which result from elastic interactions and stabilization of the nonlinear regime by the flux. This squarelike organization leads to a ratio of the positions of the two peaks in Fig. 7(c) of order $\sqrt{2}$. Finally, note that the histograms of the Voronoi tessellation do not give relevant information here, contrarily to systems with island nucleation. These results are summarized by the kinetic phase diagram in Fig. 8.

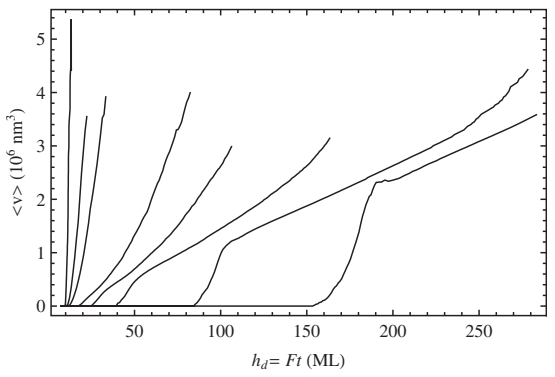

FIG. 6. Mean island volume, defined above the wetting layer, as function of the deposition height with the same convention as in Fig. 2.

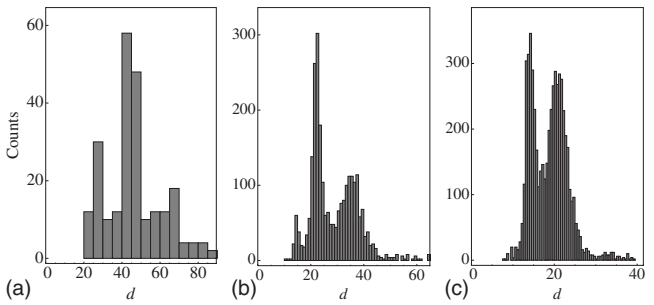

FIG. 7. Island distance distribution corresponding to Fig. 3.

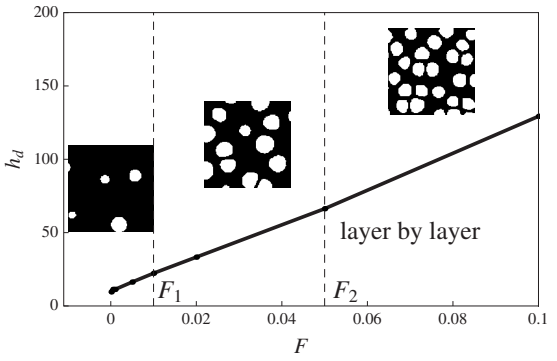

FIG. 8. Kinetic phase diagram as function of the deposited height $h_d = Ft$ and the flux. For a given flux, growth proceeds mainly layer by layer up to the dynamical critical height h_s (solid line). Above, for $F < F_1$, surface diffusion is efficient and leads to an annealinglike ripening. For $F_1 < F < F_2$, a nonconventional coarsening occurs, where the island density decreases faster than linearly. Finally, for $F > F_2$, ripening is frozen by the deposition growth, the island density is constant and highly correlated islands form ridgelike structures. The three insets correspond to the last time points of the roughness as function of time as displayed in Fig. 2 for flux values $F = 10^{-4}, 10^{-2}, 10^{-1}$ ML/s.

IV. CONCLUSION

As a conclusion, we studied the influence of a deposition flux on the growth dynamics of the elastic instability in strained crystal films. We used a continuum description accounting for wetting and elasticity where the flux arises in a nontrivial way. Once diffusion proceeded and led to island formation, we report three different nonlinear regimes, depending on the flux and characterized by different spatial ordering. At low flux, an annealinglike dynamics is at stake. Increasing the flux, we find spatial correlations where dots gather in clusters, together with a nonconventional ripening. For high flux, ripening is frozen as surface diffusion effects are inhibited by deposition growth and the dot density is maximum. The nearest-neighbor distance distribution exhibits a first peak linked to the distance between two islands in a cluster which decreases and a second one related to the cluster distance. These results indicate a way to tune different spatial ordering and are calling for experimental examination of the elastic instability. Moreover, as an extension of the present analysis, the influence of the surface energy anisotropy on the coarsening dynamics is under current investigation.

[1] V. Shchukin, N. Ledentsov, and D. Bimberg, *Epitaxy of Nanostructures* (Springer, New York, 2003); V. A. Shchukin and D. Bimberg, Rev. Mod. Phys. **71**, 1125 (1999).

[2] J. Stangl, V. Holý, and G. Bauer, Rev. Mod. Phys. **76**, 725 (2004).

[3] C. Teichert, Phys. Rep. **365**, 335 (2002).

[4] B. B. Voigtländer, Surf. Sci. Rep. **43**, 127 (2001).

[5] P. Politi, G. Grenet, A. Marty, A. Ponchet, and J. Villain, Phys. Rep. **324**, 271 (2000).

[6] A. Pimpinelli and J. Villain, *Physics of Crystal Growth* (Cambdrige University Press, Cambridge, 1998).

[7] A.-L. Barabasi and H. E. Stanley, *Fractal Concepts in Surface Growth* (Cambridge University Press, Cambridge, 1995).

[8] D. D. Vvedensky, *Frontiers in Nanoscience and Nanotechnology*, edited by A. V. Narlikar and Y. Y. Fu (Oxford University Press, Oxford, England, 2008).

[9] J. L. Gray, R. Hull, C.-H. Lam, P. Sutter, J. Means, and J. A. Floro, Phys. Rev. B **72**, 155323 (2005).

[10] A. Rastelli, M. Stoffel, J. Tersoff, G. S. Kar, and O. G. Schmidt, Phys. Rev. Lett. **95**, 026103 (2005).

[11] I. Berbezier and A. Ronda, Surf. Sci. Rep. **64**, 47 (2009).

[12] P. Sutter and M. G. Lagally, Phys. Rev. Lett. **84**, 4637 (2000).

[13] R. M. Tromp, F. M. Ross, and M. C. Reuter, Phys. Rev. Lett. **84**, 4641 (2000).

[14] I. Berbezier, A. Ronda, and A. Portavoce, J. Phys.: Condens. Matter **14**, 8283 (2002).

[15] J. A. Floro, M. B. Sinclair, E. Chason, L. B. Freund, R. D. Twesten, R. Q. Hwang, and G. A. Lucadamo, Phys. Rev. Lett. **84**, 701 (2000).

[16] H. Gao and W. Nix, Annu. Rev. Mater. Sci. **29**, 173 (1999).

[17] B. J. Spencer, P. W. Voorhees, and S. H. Davis, Phys. Rev. Lett. **67**, 3696 (1991).

[18] B. J. Spencer, S. H. Davis, and P. W. Voorhees, Phys. Rev. B **47**, 9760 (1993).

[19] Y. Xiang and W. E, J. Appl. Phys. **91**, 9414 (2002).

[20] A. A. Golovin, S. H. Davis, and P. W. Voorhees, Phys. Rev. E **68**, 056203 (2003).

[21] J.-N. Aqua, T. Frisch, and A. Verga, Phys. Rev. B **76**, 165319 (2007).

[22] M. S. Levine, A. A. Golovin, S. H. Davis, and P. W. Voorhees, Phys. Rev. B **75**, 205312 (2007).

[23] B. J. Spencer, Phys. Rev. B **59**, 2011 (1999).

[24] M. S. Leite, A. Malachias, S. W. Kycia, T. I. Kamins, R. S. Williams, and G. Medeiros-Ribeiro, Phys. Rev. Lett. **100**, 226101 (2008).

[25] M. Stoffel, A. Rastelli, J. Stangl, T. Merdzhanova, G. Bauer, and O. G. Schmidt, Phys. Rev. B **75**, 113307 (2007).

[26] Y. Tu and J. Tersoff, Phys. Rev. Lett. **93**, 216101 (2004).

[27] J. Tersoff, B. J. Spencer, A. Rastelli, and H. von Känel, Phys. Rev. Lett. **89**, 196104 (2002).

[28] M. J. Beck, A. van de Walle, and M. Asta, Phys. Rev. B **70**, 205337 (2004); G.-H. Lu and F. Liu, Phys. Rev. Lett. **94**, 176103 (2005).

[29] C. A. Haselwandter and D. D. Vvedensky, Phys. Rev. B **74**, 121408(R) (2006).

[30] B. J. Spencer, P. W. Voorhees, and S. H. Davies, J. Appl. Phys. **73**, 4955 (1993).

[31] B. Damilano, N. Grandjean, F. Semond, J. Massies, and M. Leroux, Appl. Phys. Lett. **75**, 962 (1999).

[32] B. Cho, T. Schwarz-Selinger, K. Ohmori, D. G. Cahill, and J. E. Greene, Phys. Rev. B **66**, 195407 (2002).

[33] J. Villain, A. Pimpinelli, L. Tang, and D. Wolf, J. Phys. I **2**, 2107 (1992).